Dynamic Range Enhanced Optical Frequency Domain Reflectometry Using Dual-Loop Composite Optical Phase-Locking

Yinxia Meng, Weilin Xie, *Member, IEEE*, Yuxiang Feng, Jiang Yang, Ling Zhang, Yuanshuo Bai, Wei Wei, and Yi Dong

***Abstract*—We report on a dynamic range enhanced optical frequency domain reflectometry distributed backscattering interrogator based on dual-loop composite optical phase-locked loop (OPLL). Exploiting simultaneously an acousto-optic frequency shifter based an external modulation loop and a piezo based direct modulation loop, the proposed composite OPLL allows offering a larger loop bandwidth and gain, permitting a more efficient coherence enhancement as well as sweep linearization. A high fidelity frequency sweep of ∼8.2 GHz at 164 GHz/s sweep rate is generated with a peak-to-peak frequency error as low as ∼120 kHz. It leads to a dynamic range enhancement of more than 3 dB for the measured power loss compared to the case when only piezo loop is applied. This corresponds to ∼15 km extension for the measurement range of Rayleigh backscattering without any spatial resolution penalties. Fourier transform-limited spatial resolution has been demonstrated at a range window more than about 28 times of the intrinsic coherence length of the adopted fiber laser. The proposed method provides a straightforward optimization of the real-time sweep control and is expected to be a useful tool in industrial and commercial applications.**

***Index Terms*—Fiber laser, optical phase-locked loop, optical frequency domain reflectometry, Rayleigh backscattering.**

I. Introduction

OPTICAL frequency domain reflectometry (OFDR) distributed backscattering interrogator, on account of the advantages including high spatial resolution, high sensitivity and dead-zone free interrogation, has attracted many attentions in fields of such as optical communication network monitoring [1], imaging [2], [3], and distributed sensing [4], [5]. Principally, the measurement range is mainly determined by the coherence of the probe laser while the spatial resolution is inversely proportional to the sweep range and is also theoretically dictated by the sweep nonlinearity. In this context, aiming at extending the effective measurement range, highly coherent laser sources capable of broadband linear frequency sweep has become vital. These aspects are, however, quite challenging for most of the lasers, because the trade-offs have to be concerned amongst the coherence properties, namely, the phase and frequency noise characteristics, the sweep range, and the sweep linearity for practical commercial lasers [6]–[8].

In order to cope with these difficulties, a lot of efforts have been made. Concerning the inherent restrictions for laser sources, some have focused on improving the design for the receiving and detection while efforts have also been dedicated to the enhancement of the probing source, namely, the generation of highly coherent and linear swept-frequency laser source (SFLS). In the former, nonlinear sampling relying on auxiliary interferometer (AI) that can be performed either directly acting as the acquisition trigger [9]–[12] or with re-sampling based digital processing [13]–[16], has been employed mainly to accommodate with effective sweep linearization. Though the limited measurement range in AI triggering methods due to the Nyquist theorem [11] could be mitigated in the re-sampling method, the accumulated frequency error is still problematic for long distance measurements [13], [15], [19]. In addition to the nonlinearities, different post-processing algorithms such as phase noise compensation [17] and deskew filter [19], [20] have been applied to deal with the phase noise due to the limited coherence, especially for long distance measurement. In the latter, external modulation on narrow linewidth lasers with linearly swept RF signals has been exploited, enabling measurement at tens of kilometers with the help of post compensation [18]. The coherence is directly inherited from the laser while the chirp properties are strictly dependent on the characteristics of the RF signals where wideband optical and electrical components are needed for large sweep range. To eliminate the necessitating high frequency components and to reduce the processing consumption, direct frequency modulation becomes thus popular. The inherent nonlinearities in the frequency modulation response can be mitigated a prior by the use of pre-distorted control signals. To further address this issue, optical phase-locked loop (OPLL) that permits for simultaneously sweep linearization and

Manuscript received May 31, 2021; revised June 28, 2021; accepted June 30, 2021. Date of publication July 2, 2021; date of current version July 30, 2021. This work was supported in part by the National Natural Science Foundation of China (NSFC) under Grants 61805014 and 61827807. *(Corresponding author: Weilin Xie.)*

Yinxia Meng, Weilin Xie, Yuxiang Feng, Jiang Yang, Wei Wei, and Yi Dong are with the Key Laboratory of Photonics Information Technology, Ministry of Industry and Information Technology, School of Optics and Photonics, Beijing Institute of Technology, Beijing 100081, China (e-mail: 3120185319@bit.edu.cn; wlxie@bit.edu.cn; 3120170293@bit.edu.cn; yj919@foxmail.com; weiwei@bit.edu.cn; yidong@bit.edu.cn).

Ling Zhang and Yuanshuo Bai are with the State Key Laboratory of Advanced Optical Communication Systems and Networks, Shanghai Jiao Tong University, Shanghai 200240, China (e-mail: nina_zhangling@sjtu.edu.cn; baiyuanshuo@sjtu.edu.cn).

Digital Object Identifier 10.1109/JPHOT.2021.3094330

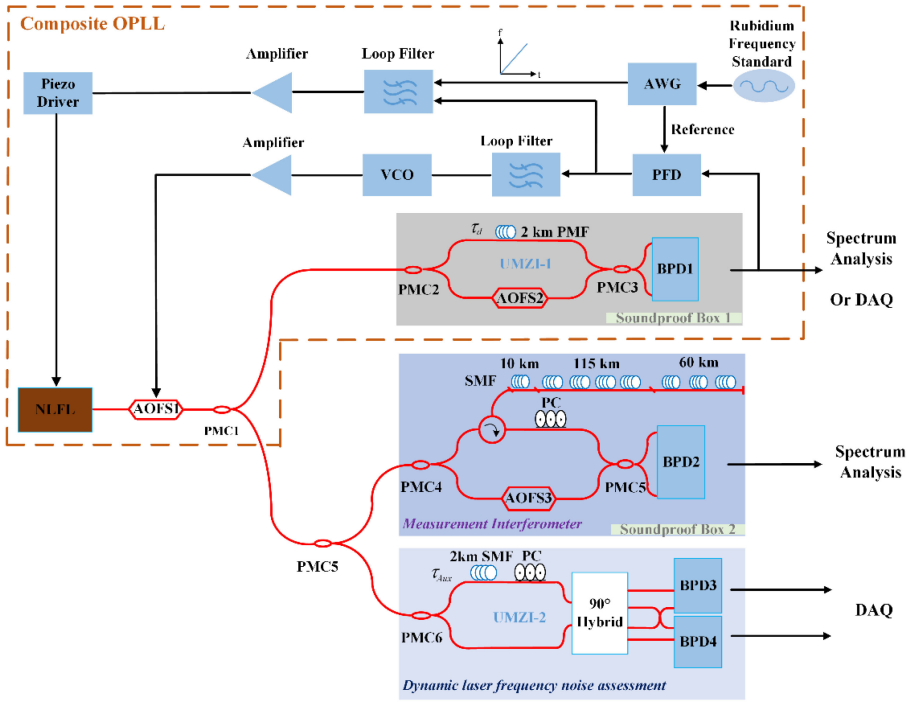

Fig. 1. Experimental setup. NLFL, narrow-linewidth fiber laser; AOFS, acousto-optic frequency shifter; PMC, polarization-maintaining coupler; BPD, balanced photodetector; DAQ, data acquisition card; PFD, phase frequency discriminator; VCO, voltage controlled oscillator; AWG, arbitrary waveform generator; PMF, polarization-maintaining fiber; SMF, single mode fiber; PC, polarization controller.

coherence enhancement have come into view [21], [22]. The effect of OPLL, nevertheless, is highly dependent on loop gain and loop bandwidth, thus fundamentally limited by loop delay. Semiconductor lasers with hybrid integration could substantially minimize the loop delay. But the residual phase errors due to the limited intrinsic coherence has yet made it difficult for long distance measurement [22], [23]. Conversely, the inherit frequency modulation response for commercial fiber lasers acts as a main limiting factor on loop bandwidth, hampering the further suppression of the residual phase error. This way, closing the gaps between locking mechanisms and loop delay would allow to take a full advantage of the high coherence for commercial fiber lasers [23], [24].

To this end, in order to improve the effective measurement range, in this paper, we present a dual-loop composite OPLL composed of two distinct opto-electronic feedback loops that permits to further exploit the potential of commercial fiber lasers. Compared with traditional single loop OPLL, it could offer a higher loop gain as well as a larger loop bandwidth, allowing for a more efficient sweep linearization and dynamic coherence enhancement while also facilitating the lock-in process. It leads to more than 3 dB dynamic range enhancement in terms of single-trip power loss, corresponding to more than 15 km round-trip measurement range extension in single-mode fiber (SMF).

II. Linearly Frequency-Swept Fiber Laser Using Dual-Loop Composite OPLL

A. Operation Principle

The proposed system is shown in Fig. 1, where a narrow linewidth fiber laser (NKT C15) is adopted with ~5 kHz linewidth around ~1554 nm measured using short-delayed self-heterodyne method as previously proposed in [25], corresponding to ~6.5 km roundtrip coherence length. An intra-cavity piezo is utilized to change the laser frequency by driving the associated piezo-electric transducer (PZT). Its output passes through an acousto-optic frequency shifter (AOFS1, Gooch & Housego, Fiber-Q) driven by a voltage-controlled oscillator (VCO) before being divided into two parts. The AOFS1 is used to alter the phase and frequency of the laser output in addition to the PZT, from which the output is regarded as the obtained phase-locked SFLS. A small portion of the power is sent into an unbalanced Mach-Zehnder interferometer (UMZI-1) to constitute a heterodyne OPLL with AOFS2 and optical fiber of delay τ_d. According to its transfer function, laser frequency fluctuations are converted into the phase variations of the beat note with a quasi-linear relation $2\pi\tau_d$ when within a certain bandwidth that is significantly smaller than the inverse of τ_d [22]. The beat note is compared at a phase-frequency discriminator (PFD) with a stable reference provided by an arbitrary waveform generator (AWG) that is synchronized to the Rubidium frequency standard. The resulting error signal is successively processed by two home-made loop filters with distinct time constants and gains to yield the feedback signals for the PZT and AOFS loops, respectively. A pre-distorted ramp signal generated by the AWG is applied in combination with the error signal for PZT loop to trigger the frequency sweep, thus minimizing the phase errors and facilitating the locking process. Taking into account their actions, the instantaneous phase of the SFLS output can be written as

$$\theta_{\nu,t} = 2\pi\left[(\nu_0 + \nu_{\mathrm{PZT},t}) + (f_{\mathrm{AOFS1}} + \delta f_{\mathrm{AOFS1},t})\right]t + \pi(\gamma + \delta\gamma_t)t^2 + \varphi_t \quad (1)$$

where υ_0, γ, $\delta\gamma_t$, and φ_t are the initial frequency, sweep rate, sweep nonlinearities, and phase noise, respectively. In the meantime, $\upsilon_{\mathrm{PZT},t}$ holds for the PZT loop induced frequency changes while f_{AOFS1} and $\delta f_{\mathrm{AOFS1},t}$ are responsible for the frequency shift and variations produced by AOFS1, respectively.

This way, the phase of the detected beat note at the balanced photodetector (BPD1) can thereby be written as

$$\begin{aligned}\theta_{beat}\sim & 2\pi(\nu_0+f_{\mathrm{AOFS1}})\tau_d+2\pi(\delta f_{\mathrm{AOFS1},t}-\delta f_{\mathrm{AOFS1},t-\tau_d}\\ &+2\pi\delta f_{\mathrm{AOFS1},t-\tau_d}\tau_d+2\pi(\nu_{\mathrm{PZT},t}-\nu_{\mathrm{PZT},t-\tau_d})t\\ &+f_{\mathrm{AOFS2}})t+2\pi\nu_{\mathrm{PZT},t-\tau_d}\tau_0+\pi(\delta\gamma_t-\delta\gamma_{t-\tau_d})t^2\\ &+2\pi(\gamma+\delta\gamma_{t-\tau_d})\tau_d t-\pi(\gamma+\delta\gamma_{t-\tau_d}){\tau_d}^2+\Delta\varphi_{t,\tau_d}\end{aligned} \tag{2}$$

where $f_{\mathrm{AOFS2}}=f_{\mathrm{AOFS1}}$ is the operating frequency for AOFS2. In free-running case, except for the constant phase terms produced by υ_0 and AOFS1 as expressed in the first term in Eq. (2), the frequency sweep and the other time-varying terms can be resorted out to the contributions from sweep nonlinearities, laser phase noise, and the actions induced by both the PZT and AOFS1. In closed-loop case, according to the integral loop operation, theoretically, the PZT and AOFS1 induced phase and frequency changes should be able to compensate for the variations as a consequence of the nonlinearities and laser phase noise. This way, neglecting those constant phase terms, the instantaneous phase of the RF beat note should be equal to that of the reference as illustrated in the following

$$2\pi f_{\mathrm{ref}}t=2\pi(f_{\mathrm{AOFS2}}+\gamma\tau_d)t \tag{3}$$

where f_{ref} is the frequency of the reference. It can be directly inferred that with a proper choice for the reference frequency, it will lead to an ideal linear frequency sweep, provided infinite loop gain and bandwidth. Nevertheless, several constrains need to be accounted for from a practical point of view. The effect of OPLL is largely determined by the loop gain and bandwidth according to loop control theory [22]. As aforementioned, the delay of the UMZI-1 acts as a limiting factor in loop characteristics. Besides, it is also dictated by the modulation response of the actuators and their associated loop delays. Therefore, the UMZI-1 delay should be decided in a manner that it is able to provide as large as possible discrimination gain while maximizing the loop bandwidth. In current demonstration, the PZT is able to provide a large gain within a restricted bandwidth no more than a few tens of kHz owing to its natural resonance. Meanwhile, the response time of commercial AOFS could achieve a few tens of ns with MHz modulation depth, potentially allowing for a broader loop bandwidth up to MHz range. Taking into consideration all these aspects, 2 km fiber delay is chosen for UMZI-1, corresponding to $\tau_d=10\,\mu$s. This way, such composite OPLL permits efficient exploitation for the potentials of the fiber laser. To minimize the deterioration induced by the environmental perturbations, the UMZI-1 is placed in a homemade wooden soundproof box.

The fiber under test (FUT) consisting of several sections of spooled fiber is connected via a circulator. The backscattered lights travel through a polarization controller to maximize the interference efficiency. From a practical viewpoint, a polarization diversity receiver will be more efficient to mitigate the polarization fading and will be adopted in the future. It converges with the reference signal from the other arm with an AOFS3 induced $40\ \mathrm{MHz}$ frequency shift before feeding into BPD2. In order to avoid the impairment in spatial resolution due to the environmental disturbances along the FUT [24], the FUT is placed in soundproof box-2. At the same time, a short-delayed UMZI-2 with a 2 km fiber delay, corresponding to $\tau_{Aux}=10\ \mu$s, and a 90° optical hybrid are used for dynamic laser frequency noise assessment.

B. Effect of OPLL in Static and Dynamic Operations

Firstly, we evaluate the effect of phase-locking in static (fixed-frequency) operation using a real-time spectrum analyzer (RSA). The beat notes at BPD1 in single-(only the PZT loop) and dual-loop (composite OPLL with both the PZT and AOFS loops) cases, respectively, are shown in Fig. 2. Though these two loops can either achieve a phase-locking, the latter shows a more prominent performance. Not only the in-band noise of the beat note is further suppressed by almost 10 dB with an extended loop bandwidth up to $\sim$80 kHz compared to that of $\sim$9 kHz in single-loop case, but also the bumps around the offset of $10\sim 40$ kHz have been additionally suppressed by more than 15 dB in dual-loop case. Meanwhile, the peak carrier-to-noise ratio (CNR) reaches up to $\sim$60 dB, which is $\sim$15 dB higher than that of the single-loop case. Moreover, it can be found that the steep truncations appeared at the offset of $\sim$40 kHz in single-loop is probably attributed to the inherit resonance in the frequency modulation response of PZT. The deterioration in phase margin because of this phenomenon could be mitigated to some extent thanks to the fast frequency modulation response of AOFS1 in dual-loop case.

In dynamic (swept-frequency) operation, being subjected to the inherent restriction for the fiber laser, the sweep range and period are set to as 8.2 GHz and 50 ms, respectively, corresponding to a sweep rate of 164 GHz/s. As indicated in Fig. 3, in free-running case a large noise bump due to the nonlinearities and phase noises have emerged in the beat note spectrum. While in close-loop cases, clear coherent beat note peaks are obtained in accordance with the rectified linear frequency sweep and enhanced coherence property. Obviously, the effect of dual-loop composite OPLL has been well confirmed as manifested by the effective suppression for the close-in noise pedestal as well as for the noise protuberance around $10\sim 40$ kHz in single-loop case. Therefore, it is convinced the dual-loop composite OPLL could allow for an essential improvement for the dynamic coherence of the SFLS.

It is noted that the extra bumps emerged when approaching the loop bandwidth ($\sim$ 80 kHz) in dual-loop case imply a sharply degraded phase margin around those frequencies. This is probably attributed to the UMZI delay which in principally imposes a strict limit in the loop bandwidth, which must be carefully accounted for when designing the dual-loop composite OPLL.

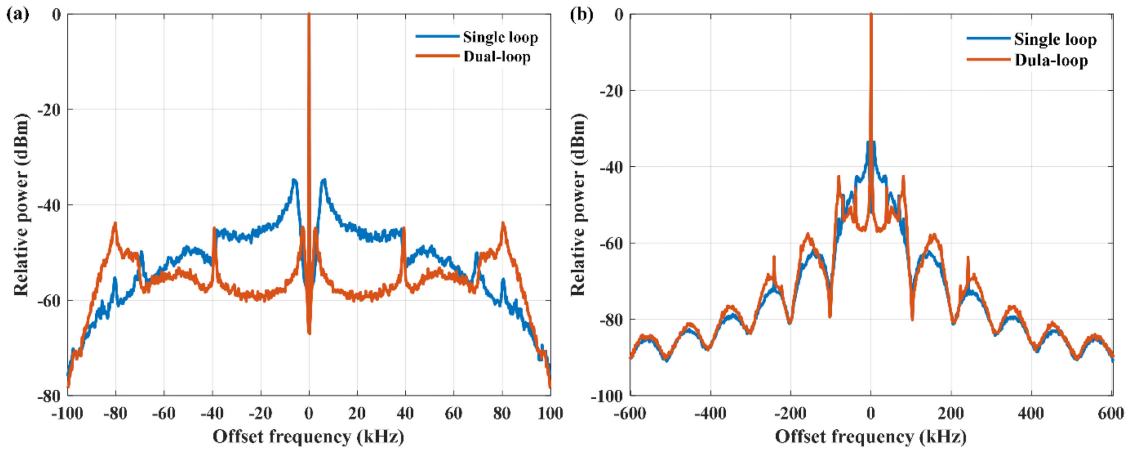

Fig. 2. Beat notes at BPD1 of phase-locking in static (fixed-frequency) operation at frequency offset ranges of (a) ±100 kHz; (b) ±600 kHz.

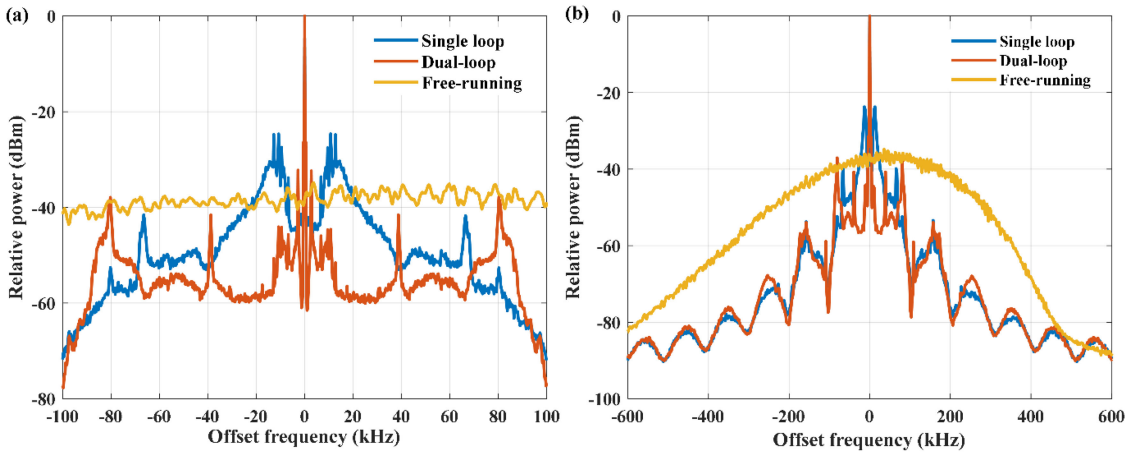

Fig. 3. Beat notes at BPD1 when the laser frequency is sweeping over 8.2 GHz in 50 ms in different cases at frequency offset ranges of (a) ±100 kHz; (b) ±600 kHz.

C. Characterization of the Generated SFLS

To analyze the sweep characteristics, the instantaneous optical frequency is calculated relying on the relation given by the transfer function of UMZI where the instantaneous phase changes of the beat note is extracted using Hilbert transform. The results in different cases are shown in Fig. 4. Compared to the serious nonlinearities and large frequency error in free-running case, in both single and dual-loop cases, significantly improved linearity has been attained. It is worth noting that a slight temporal shift can be observed between the two locked cases, especially in the beginning of the sweep, inferring a shorter transition from the static to sweep operation in dual-loop case. This is mainly due to the large loop bandwidth, namely the fast loop response enabled by the composite OPLL that permits to avoid the underlying phase slips induced by excessive accelerations in the start of the sweep and thus facilitate the locking process.

A linear fitting is carried out to extract the frequency error during the sweep as described in Fig. 5 for all the cases. Despite the large frequency deviations reaching up to about GHz range (see Fig. 5(a)) in free-running case, we achieved a peak-to-peak frequency error as low as ∼120 kHz in dual-loop case with a non-trivial enhancement than that in single-loop case (about 300 kHz) as compared in Fig. 5(b). In addition, the transition from static to dynamic, namely, fixed- to swept-frequency operation has also been facilitated as the peak frequency error in the

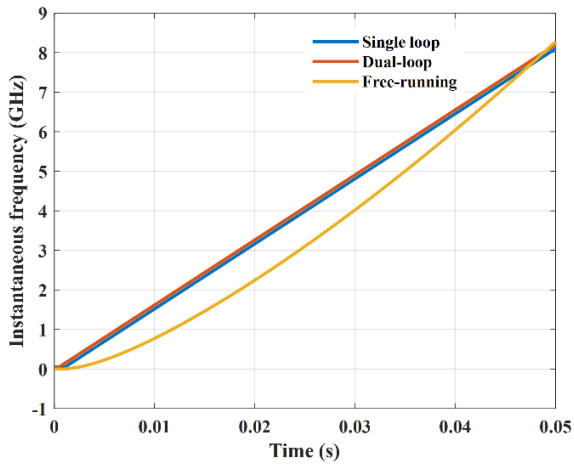

Fig. 4. The instantaneous frequency of the SFLS output in different cases.

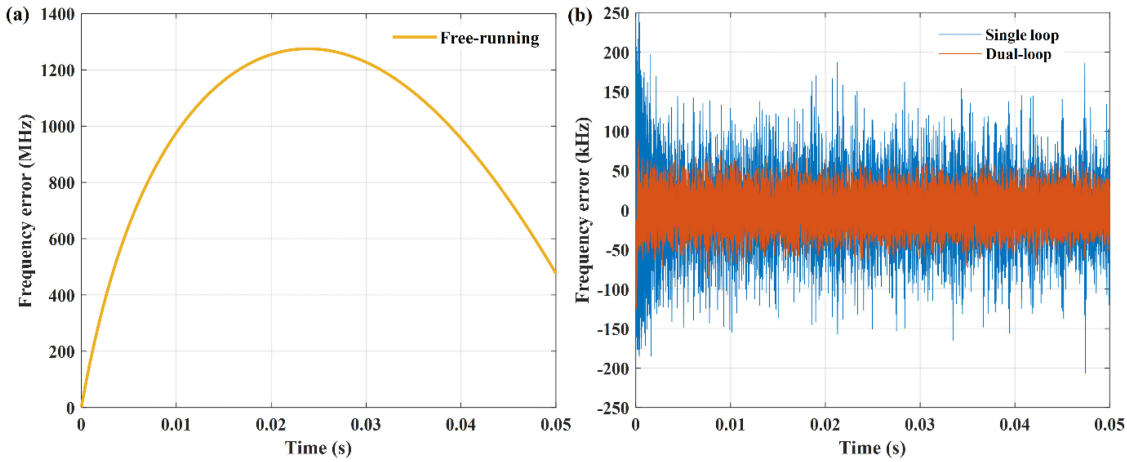

Fig. 5. Frequency error when the SFLS is sweeping over 8.2 GHz in 50 ms in different cases. (a) Free-running case; (b) Single- and dual-loop cases.

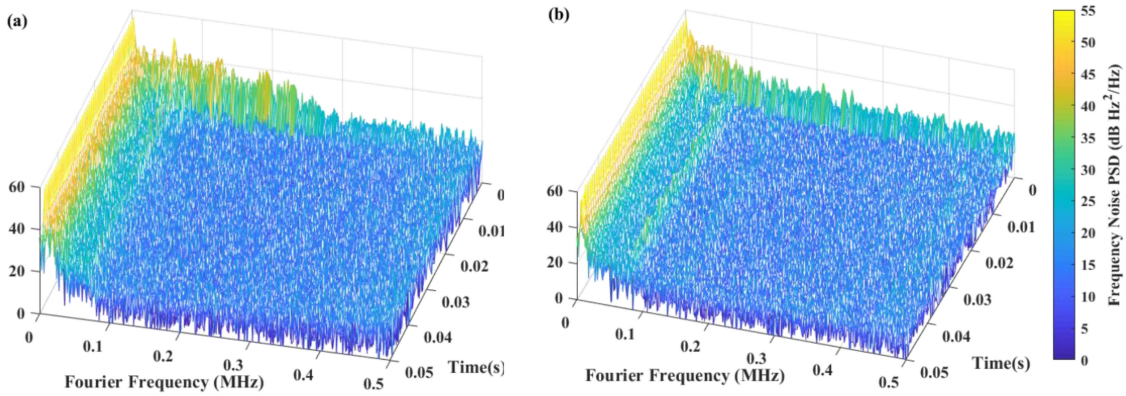

Fig. 6. Dynamic frequency noise PSD measured from the UMZI-2, the SFLS is sweeping over 8.2 GHz in 50 ms. (a) Single- (b) Dual-loop cases.

beginning of the sweep is significantly reduced, which in turn testifies to the results presented in Fig. 4.

D. Dynamic Laser Frequency Noise in Out-of-loop Assessment

The laser frequency noise spectrum is presented by using an auxiliary UMZI-2 as shown in the bottom of Fig. 1 for an out-of-loop assessment to provide a finer insight for the dynamics of the OPLL during the sweep. The outputs from the 90° optical hybrid are sampled by a data acquisition card (DAQ) to extract the phase variations, thus the laser frequency fluctuations. The corresponding dynamic frequency noise power spectral density (PSD) is calculated by analyzing the sliced temporal data [25] using a short-time Fourier transform (STFT), as visualized in Fig. 6 with the sliced temporal interval chosen as 1 ms.

In the transition when the laser hastily alters from the static state to the dynamic frequency sweep process, a highly distorted frequency noise PSD can be observed since the loop urges to enter the locking state. Such transition in single loop case has almost occupied the first 1 ms while that in dual-loop case has been accomplished much shorter than 1 ms, not to mention the more effective noise suppression in dual-loop case as discussed previously. Once the laser steadily enters the closed-loop operation, the frequency noise PSD within the loop bandwidth stays relatively stable throughout the entire sweep processes, indicating an evident improvement for the dynamic coherence towards a highly linearized and coherent SFLS.

III. Measurement of Power Loss in OFDR Verification

The FUT is composed of several spools of SMF, where we set three reflection points with angle polished connector (APC) at 10 km and 125 km and a polished connector (PC) at the end of 185 km, respectively. When performing Fourier analysis to locate the reflection events, Hanning window is applied in spectrum analysis with 10 times average of the trace so as to reduce the fluctuations in Rayleigh backscattering (RBS). As described in Fig. 7, at the distance of ∼10 km, we could see evident reflection events in either single or dual-loop cases. The spatial resolution of the reflection peaks in the two cases are 2.9 cm and 2.8 cm, respectively. In our measurement, the spatial resolution is actually limited by the analysis window of the RSA rather than that determined by the 8.2 GHz sweep range. When it increases to ∼125 km, the spatial resolution in both cases show similar degradations. At a longer distance of ∼185 km,

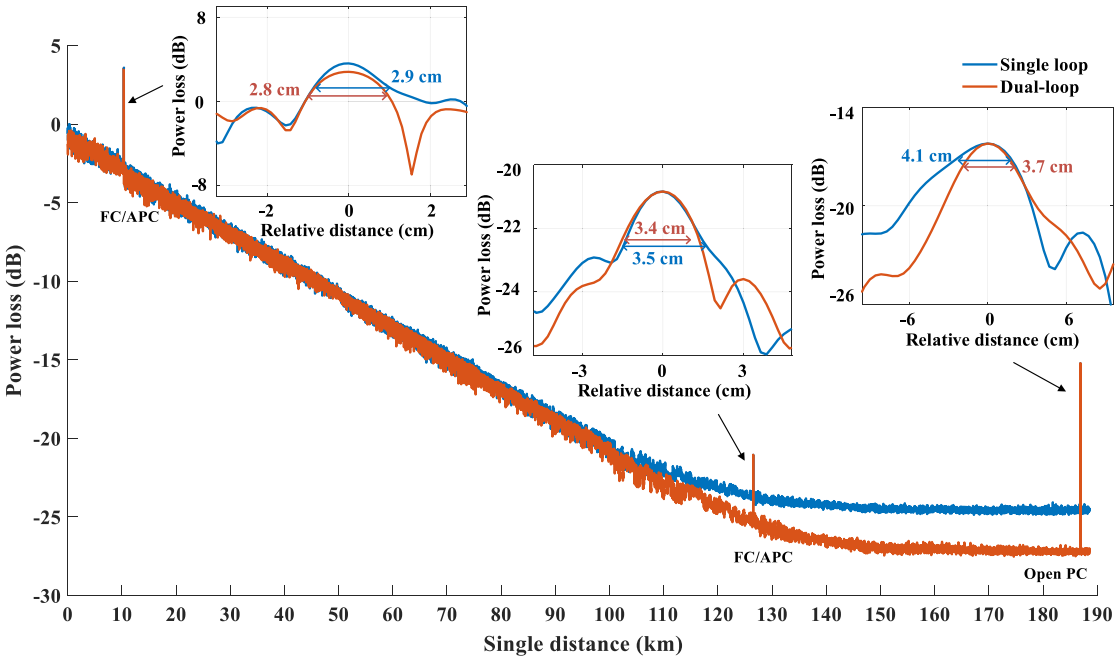

Fig. 7. Measurement results of OFDR trace. Inset: details of the peaks at 10 km, 125 km and 185 km. Blue curve: single-loop case; red curve: dual-loop case.

the decrease in spatial resolution is nearly moderate in both cases. This deterioration in spatial resolution when approaching and exceeding the coherence length is mainly attributed to the residual phase noise and nonlinearities. It is worth noting that the sound-proof box-2 is applied in order to mitigate the influences due to the fluctuations of the fiber links.

More importantly, the experiment results show that the dual-loop case exhibits a better capability to suppress the phase noise of the fiber laser than the single loop case. We achieved more than 3 dB improvement in dynamic range, corresponding to ∼15 km extension in RBS measurement range without sacrificing the spatial resolution, which has been demonstration in the long-distance test of the proposed OFDR system.

IV. Conclusion

In conclusion, we proposed an effective scheme to enhance the dynamic range for an OFDR distributed backscattering interrogator based on a dual-loop composite OPLL. Consisting of an external AOFS and an intracavity PZT, it enables a more efficient linearization and dynamic coherence enhancement. It allows for fully exploring for the potential of commercial fiber lasers, achieving highly coherent SFLS with ∼8.2 GHz sweep range at 164 GHz/s sweep rate with ∼120 kHz peak-to-peak frequency error. We achieved more than 3 dB improvement on dynamic range of power loss in OFDR measurement, corresponding to ∼15 km RBS measurement range extension compared with single-loop case without any spatial resolution penalty. This is about 28 times than that of the intrinsic round-trip coherence length. It provides a promising direction for the dynamic coherence towards a highly linearized and coherent laser source in real-time sweep control technique.

References

[1] J. P. Von der Weid and R. Passy, "On the characterization of optical fiber network components with optical frequency domain reflectometry," *J. Lightw. Technol.*, vol. 15, no. 7, pp. 1131–1141, Jul. 1997.
[2] J. Buck and A. Malm, "High-resolution 3D coherent laser radar imaging," in *Proc. SPIE*, vol. 6550, 2007, Art. no. 655002.
[3] J. Zheng, "Optical frequency-modulated continuous-wave interferometers," *Appl. Opt.*, vol. 45, no. 12, pp. 2723–2730, 2006.
[4] M. Froggatt and J. Moore, "High-spatial-resolution distributed strain measurement in optical fiber with Rayleigh scatter," *Appl. Opt.*, vol. 37, no. 10, pp. 1735–1740, Apr. 1998.
[5] J. Song and W. Li, "Long-range high spatial resolution distributed temperature and strain sensing based on optical frequency-domain reflectometry," *IEEE Photon. J.*, vol. 6, no. 3, Jun. 2014, Art. no. 6801408.
[6] E. Leviatan and A. Eyal, "High resolution DAS via sinusoidal frequency scan OFDR (SFS-OFDR)," *Opt. Exp.*, vol. 23, no. 26, pp. 33318–33334, Sep. 2015.
[7] D. P. Zhou and Z. Qin, "Distributed vibration sensing with time-resolved optical frequency-domain reflectometry," *Opt. Exp.*, vol. 20, no. 12, pp. 13138–13145, Jun. 2012.
[8] B. Soller and D. Gifford, "High resolution optical frequency domain reflectometry for characterization of components and assemblies," *Opt. Exp.*, vol. 13, no. 2, pp. 666–674, Nov. 2005.
[9] M. Kobayashi and K. Takada, "Optical-frequency encoder using polarization-maintaining fiber," *J. Lightw. Technol.*, vol. 8, pp. 1697–1702, 1990.
[10] K. Takada, "High-resolution OFDR with incorporated fiber-optic frequency encoder," *IEEE Photon. Technol. Lett.*, vol. 4, no. 9, pp. 1069–1072, Sep. 1992.
[11] U. Glombitza and E. Brinkmeyer, "Coherent frequency-domain reflectometry for characterization of single-mode integrated-optical waveguides," *J. Lightw. Technol.*, vol. 11, pp. 1377–1384, Aug. 1993.
[12] K. Iiyama and M. Yasuda, "Extended-range high-resolution FMCW reflectometry by means of electronically frequency-multiplied sampling signal generated from auxiliary interferometer," *IEICE Trans. Electron.*, vol. E89C, pp. 823–829, 2006.
[13] K. Yuksel and M. Wuilpart, "Analysis and suppression of nonlinear frequency modulation in an optical frequency-domain reflectometer," *Opt. Exp.*, vol. 17, no. 7, pp. 5845–5851, Mar. 2009.
[14] T. J. Ahn and J. Y. Lee, "Suppression of nonlinear frequency sweep in an optical frequency-domain reflectometer by use of hilbert transformation," *Appl. Opt.*, vol. 44, no. 35, pp. 7630–7634, Dec. 2005.

[15] S. Vergnole and D. Lévesque, "Experimental validation of an optimized signal processing method to handle non-linearity in swept-source optical coherence tomography," *Opt. Exp.*, vol. 18, no. 10, pp. 10446–10461, Feb. 2010.

[16] K. K. H. Chan and S. Tang, "High-speed spectral domain optical coherence tomography using non-uniform fast Fourier transform," *Bio. Opt. Exp.*, vol. 1, no. 5, pp. 1310–1319, Sep. 2010.

[17] F. Ito and X. Fan, "Long-range coherent OFDR with light source phase noise compensation," *J. Lightw. Technol.*, vol. 30, no. 8, pp. 1015–1024, Oct. 2012.

[18] Y. Koshikiya and X. Fan, "Long range and cm-level spatial resolution measurement using coherent optical frequency domain reflectometry with SSB-SC modulator and narrow linewidth fiber laser," *J. Lightw. Technol.*, vol. 26, no. 18, pp. 3287–3294, Sep. 2008.

[19] Z. Ding and X. S. Yao, "Compensation of laser frequency tuning nonlinearity of a long range OFDR using deskew filter," *Opt. Exp.*, vol. 21, no. 3, pp. 3826–3834, Nov. 2013.

[20] Y. Du *et al.*, "Method for improving spatial resolution and amplitude by optimized deskew filter in long-range OFDR," *IEEE Photon. J.,* vol. 6, no. 5, Oct. 2014, Art. no. 7902811.

[21] N. Satyan and A. Vasilyev, "Precise control of broadband frequency chirps using optoelectronic feedback," *Opt. Exp.*, vol. 17, no. 18, pp. 15991–15999, Aug. 2009.

[22] W. Xie and Q. Zhou, "Fourier transform-limited optical frequency-modulated continuous wave interferometry over several tens of laser coherence lengths," *Opt. Lett.*, vol. 41, no. 13, pp. 2962–2965, Jul. 2016.

[23] Q. Zhou and W. Xie, "Compensation of phase error in optical frequency-domain reflectometry using delay-matched sampling" *Opt. Eng.*, vol. 53, 2014, Art. no. 074103.

[24] Y. Feng and W. Xie, "High-performance optical frequency-domain reflectometry based on high-order optical phase-locking-assisted chirp optimization," *J. Lightw. Technol.*, vol. 38, no. 22, pp. 6227–6236, Nov. 2020.

[25] Q. Zhou and J. Qin, "Dynamic frequency-noise spectrum measurement for a frequency-swept DFB laser with short-delayed self-heterodyne method," *Opt. Exp.*, vol. 23, no. 22, pp. 29245–29257, Nov. 2015.